

## Article

# Enhancing the Physical, Thermal, and Mechanical Responses of a Mg/2wt.%CeO<sub>2</sub> Nanocomposite Using Deep Cryogenic Treatment

Shwetabh Gupta <sup>†</sup>, Gururaj Parande , Khin Sandar Tun  and Manoj Gupta <sup>\*</sup>

Department of Mechanical Engineering, National University of Singapore, 9 Engineering Drive 1, Singapore 117575, Singapore

\* Correspondence: mpegm@nus.edu.sg; Tel.: +65-6516-6358

† Current address: Blackett Laboratory, Imperial College, London SW7 2AZ, UK.

**Abstract:** Deep cryogenic treatment has shown promise as a facile method of increasing the characteristics of many materials including alloys of iron, aluminum, and magnesium. However, there have not been any prior studies on its effect on the microstructure and thermal and mechanical properties of magnesium-based nanocomposites. In this study, a Mg/2wt.%CeO<sub>2</sub> nanocomposite was processed using disintegrated melt deposition processing coupled with hot extrusion, followed by cryogenic treatment in liquid nitrogen for 24 h. The characterization results show increases in density (reduction in porosity), ignition temperature, compressive yield strength, compressive ductility, and microhardness. This study, for the first time, shows the significant relevance of deep cryogenic treatment in enhancing an array of properties of a magnesium-based nanocomposite that may be catalytic in improving its application spectrum.

**Keywords:** magnesium; metal matrix composite; nanocomposite; cryogenic treatment; mechanical properties; thermal response



**Citation:** Gupta, S.; Parande, G.; Tun, K.S.; Gupta, M. Enhancing the Physical, Thermal, and Mechanical Responses of a Mg/2wt.%CeO<sub>2</sub> Nanocomposite Using Deep Cryogenic Treatment. *Metals* **2023**, *13*, 660. <https://doi.org/10.3390/met13040660>

Academic Editors: Mieczyslaw Jurczyk and Yong Zhang

Received: 5 December 2022

Revised: 7 February 2023

Accepted: 21 March 2023

Published: 26 March 2023



**Copyright:** © 2023 by the authors. Licensee MDPI, Basel, Switzerland. This article is an open access article distributed under the terms and conditions of the Creative Commons Attribution (CC BY) license (<https://creativecommons.org/licenses/by/4.0/>).

## 1. Introduction

Cryogenic treatment, in the context of conventional materials science, involves subjecting metallic materials to sub-zero temperatures [1–3]. Cryogenic treatment has been used for almost 300 years and has been primarily explored to increase the hardness and wear resistance of steels [4,5]. Previous studies indicate that cryogenic treatment has the potential to increase the reliability and life of steel components by as much as four times [1,3,6]. Recently, there have been some reports on the effect of cryogenic treatment on the properties of magnesium alloys. Dong et al. [7] studied the effect of liquid nitrogen treatment for 24 h, 48 h and 144 h on the mechanical properties of Mg-2Nd-4Zn alloy. The yield strength and ultimate strength were found to be similar pre- and post-liquid nitrogen treatment at all conditions. However, the ductility of the alloy progressively improved from day 1 to day 6. Jiang et al. [8] studied the effect of cryogenic treatment of hot-rolled AZ31 alloy for 2, 24, and 48 h. The yield strength and ductility improved until 24 h, followed by a slight dip for 48 h. The ultimate strength showed no particular trend. Lin et al. [9] studied the effect of liquid nitrogen exposure for 16 h on ZK60 alloy. A slight improvement in the yield and ultimate strengths was reported and an appreciable increase in the ductility was reported.

To mitigate climate changes arising from the unprecedented global warming occurring in the 21st century, multi-pronged approaches have been attempted. One of the approaches is reducing the weight of transportation devices [10–12]. This has triggered the replacement of conventional materials such as steel and aluminum with magnesium-based materials. Magnesium (Mg) can provide up to 33% weight saving over aluminum and 75% over steel [13]. Such weight reduction is crucial in cutting down on fossil fuel consumption, particularly in the transportation sector (road, sea, trains, aerospace, and space) [10–12].

Magnesium-based materials are also targeted for sports and electronic sectors to minimize weight and address ergonomic issues. However, the current literature on the cryogenic treatment of magnesium-based alloys is limited so far [1,2]. Investigations have shown that cryogenic treatment can modify the microstructure [1,2,8,14] and properties of magnesium alloys [8,14]. The enhancement in characteristics of magnesium-based materials is very important as the properties of commercially available magnesium-based materials are limited when compared to the aluminum-based materials which they intend to replace for a significant weight reduction (~33%). Many methods have been used in recent times to enhance the properties of magnesium-based materials to make them useful in a wider spectrum of applications, thus paving the way to reduce the use of neurotoxic aluminum-based materials. These methods primarily include (a) the development of new Mg-based materials such as multicomponent alloys and composites; (b) microstructural tailoring through novel and new primary and secondary processing methods; and (c) through judicious selection of traditional heat treatment procedures that include the heating of materials at different times and temperatures beyond room temperature. Among the new materials, magnesium-based nanocomposites have emerged strongly over the last 20 years [12–15]. Numerous studies have shown that different types of reinforcements (oxides, carbides, borides nitrides, and C families) when judiciously integrated with pure Mg and Mg alloys, particularly at nano-length scale, have the capability to improve [16] (a) elastic modulus, (b) damping, (c) ignition temperature, (d) strength, (e) ductility, (f) fatigue response, (g) creep resistance, (h) machining, (i) dry and wet corrosion resistance, and biocompatibility. All these desirable results are obtained at almost no weight penalty as the amount of nano-reinforcement is typically restricted to a range between 0.5 and 3% [16] by volume, unlike micron-size reinforcements where the amount typically incorporated is in the range of 10–30% [12]. The present study was therefore directed at magnesium-based nanocomposites.

There is no work that has been carried out thus far in exploring deep cryogenic treatment to tailor the microstructure and further enhance the properties of magnesium-based nanocomposites. Accordingly, the present study particularly focuses on exposing an extruded Mg/2wt.%CeO<sub>2</sub> nanocomposite to liquid nitrogen (deep cryogenic treatment) and investigating its effect on the microstructure and physical, thermal, and mechanical responses. An attempt is made to interrelate the processing, microstructure, and properties of Mg/2wt.%CeO<sub>2</sub> nanocomposite.

## 2. Materials and Methods

### 2.1. Materials Processing

Pure Mg (99.9% purity) turnings supplied by ACROS Organics, USA, and CeO<sub>2</sub> nanoparticles in the size range of 15–30 nm supplied by Alfa Aesar, USA, were used as the raw materials. Pure Mg was used as a base to isolate the effect of cryogenic treatment on the properties of the materials as, in the case of Mg-based alloys, the improvement or decrement in properties can be attributed to various reasons, including precipitation and secondary phase formation, which may be affected by cryogenic treatment [1–3]. Hence, pure Mg was used as a base to understand the suitability of the deep cryogenic treatment and reinforcement addition. Further, the choice of CeO<sub>2</sub> in nanolength scale was prompted based on an earlier study where nano reinforcement displayed a more pronounced effect in improving the mechanical properties of magnesium in comparison with sub-micron and micron sizes [17]. Disintegrated melt deposition (DMD) method was used for primary processing. A detailed description of the DMD process can be found in the following reference [15]. The choice of DMD for primary processing was made due to its capability to harness the advantages of low-cost and scalable stir-casting, as well as being able to utilize the scientifically innovative spray atomization and deposition method [18]. DMD method has been developed as environmentally friendly method that (a) does not use strong greenhouse gases such as SF<sub>6</sub> and, instead, Ar/N<sub>2</sub> gases are used as protective cover; (b) does not use flux that can later entrap in solidified metal and therefore need skimming; and (c) poured yield typically exceeds 90% as the shrinkage cavity is shallow. Mg turnings and CeO<sub>2</sub> nanoparticles were placed in a

sandwich arrangement in a graphite crucible and superheated to a temperature of 750 °C in a protective argon atmosphere. The melt was stirred for 2 min 30 s using a mild steel impeller blade at 460 rev·min<sup>-1</sup> for the uniform distribution of the nanoparticles in the Mg melt and temperature homogenization. The melt was subsequently poured into a steel mold to obtain a solid ingot of 40 mm diameter. The Mg and Mg-CeO<sub>2</sub> ingots were machined, soaked at 400 °C for 1 h, and hot extruded at 350 °C using an extrusion ratio of 20.25:1 to obtain cylindrical rods of 8 mm diameter. Deep cryogenic treatment (DCT) was performed on cut samples from the extruded section by immersing them in a Dewar containing liquid nitrogen (LN) for 24 h at -196 °C (77 K). The immersion time was chosen based on the recommendation made in the open literature [1–3].

## 2.2. Characterization

The experimental densities of the extruded samples were calculated using Archimedes' principle before and after DCT treatment. Five samples were used to measure the densities of the materials using an A&D GH-252 electronic balance with an accuracy of ±1 mg. The theoretical density of the Mg/2wt.%CeO<sub>2</sub> composite was obtained by the rule of mixtures, from the theoretical densities of Mg (1.738 g·cm<sup>-3</sup>) and CeO<sub>2</sub> (7.132 g·cm<sup>-3</sup>), respectively. Porosity values were calculated by comparing the measured and theoretical densities.

Grain size analysis was performed using the Leica metallographic optical microscope and JEOL JSM-6010 Scanning Electron Microscope (SEM). Samples were ground, polished, and etched for 30 s to reveal the grains and particle distribution in the microstructure. Oxalic acid (10% aqueous oxalic acid + 3 drops of ethylene glycol + de-ionized water) was used as the etchant. X-ray diffraction (XRD) studies were performed along the longitudinal direction using the Shimadzu LAB-XRD-6000 automated spectrometer with Cu K<sub>α</sub> radiation of 0.154056 nm wavelength and a scan speed of 2 °C·min<sup>-1</sup>.

Differential scanning calorimetry (DSC) analysis was performed using the Shimadzu DSC-60 instrument to understand the effect of DCT on the thermal behavior of samples. Parameters including an argon gas flow rate of 25 mL·min<sup>-1</sup> with a heating rate of 5 °C·min<sup>-1</sup> and a temperature range of 30–600 °C were used. Thermogravimetric analysis (TGA) was conducted to ascertain the ignition temperature of the samples. Purified air with a flow rate of 50 mL·min<sup>-1</sup> and a heating rate of 10 °C·min<sup>-1</sup> within a temperature range from 30 to 1000 °C were used.

Ignition temperatures of pure Mg and Mg/2wt.%CeO<sub>2</sub> composites before and after DCT were determined using a Thermo Gravimetric Analyzer. Parameters including a heating rate of 10 °C·min<sup>-1</sup> and purified air with a flow rate of 50 mL·min<sup>-1</sup> in a temperature range from 30 to 1000 °C were used.

Microhardness was measured using a Shimadzu-HMV automatic digital microhardness tester equipped with a Vickers indenter. As per ASTM standard E384-08, a load of 245.2 mN with a dwell time of 15 s was used for each indentation. A minimum of 20 readings were taken per sample. Quasi-static compression testing was conducted using a MTS E44 fully automated servo-hydraulic mechanical testing machine at a strain rate set at  $5 \times 10^{-3}$  min<sup>-1</sup>. A minimum of three samples of 8 mm diameter each with a length-to-diameter (L/D) ratio of 1 were studied. Post-fracture examination was conducted using SEM, and the representative images were analyzed to provide insight into fracture mechanisms.

## 3. Results and Discussion

### 3.1. Macrostructural Characterization

Macrostructural analysis conducted on as-cast samples revealed no observable macroscopic defects such as abnormal surface distortion, macropores, or cracking. After extrusion, there were no observable structural defects present on the extruded rods, suggesting the feasibility of primary and secondary processing of Mg-2CeO<sub>2</sub> composites using the currently utilized parameters.

### 3.2. Density and Porosity Measurements

Table 1 shows the results of density measurements conducted on nanocomposite samples before and after DCT. The results show that the porosity level remained less than 2%, suggesting the near-net-shape capability of the processing methodology used in the present study. The deep cryogenic treatment of the as-extruded nanocomposite sample led to a reduction in porosity (increase in density) by ~44% (from 0.9764% to 0.5445%). This can be attributed to (a) the large compressive stresses [1,8,14] that set in during DCT leading to inward microscopic deformation of pores; and (b) the capability of pores to serve as a sink for dislocations that are typically and copiously generated during DCT [1,14].

**Table 1.** Results of density and porosity of Mg/2wt.%CeO<sub>2</sub> composite before and after DCT.

Material	Theoretical Density (g.cm <sup>-3</sup> )	Before DCT		After DCT	
		Measured Density (g.cm <sup>-3</sup> )	Porosity (%)	Measured Density (g.cm <sup>-3</sup> )	Porosity (%)
Pure Mg <sup>a</sup>	1.7380	1.732 ± 0.0005	0.319	-	-
Mg/2wt.%CeO <sub>2</sub> (AE)	1.7648	1.745 ± 0.002	1.099	-	-
Mg/2wt.%CeO <sub>2</sub> (AE + LN)	1.7648	1.7476 ± 0.0009	0.9764	1.755 ± 0.002	0.5545

<sup>a</sup> Values generated in the laboratory using similar raw materials and processing methods [16]. Note: AE—As Extruded; AE + LN—As Extruded + Liquid Nitrogen Treatment.

### 3.3. Microstructure

The results of grain size measurement are shown in Table 2. The results reveal no change in grain size (considering standard deviation) and its aspect ratio following DCT. The microstructure did not reveal the presence of twins within the magnification/resolution range of scanning electron microscopy after DCT, which otherwise is commonly reported by investigators [8,14]. The results suggest that this may be attributed to the relatively small grain size of the samples before and after DCT (~2–3 μm range) [17,19]. In a study conducted by Tsai and Chang [17], the grain size effect on the twinning was clearly presented. They indicated that only 1.61% of the grains were twinned in the 3–7 μm size range while 28.6% of grains twinned in the 35–39 μm size range. In yet another study [19], investigators reported a critical grain size of about 2.7 μm, below which activation of twinning becomes difficult and deformation proceeds primarily through dislocation slip. As the grain size of the samples in the present study remained lower than 3 μm, it is expected that twinning or twinned grains' presence will be negligible [17–19]. Notably, higher stress is required to twin the grains of smaller size [17] and the stresses generated before and after DCT were not enough to twin the grains in the samples used in the present study.

**Table 2.** Results of grain size analysis for Mg/2wt.%CeO<sub>2</sub> composite before and after DCT.

Material	Grain Size (μm)	Aspect Ratio
Pure Mg <sup>a</sup>	21.8 ± 5.0	1.4 ± 0.2
Mg/2wt.%CeO <sub>2</sub> (AE)	2 ± 0.6	1.4 ± 0.3
Mg/2wt.%CeO <sub>2</sub> (AE + LN)	2.8 ± 0.6	1.2 ± 0.3

<sup>a</sup> Values generated in the laboratory using similar raw materials and processing methods [16].

The distribution of nano-CeO<sub>2</sub> following extrusion and DCT remained similar. CeO<sub>2</sub> particles were mostly distributed at the grain boundaries and appeared to be in small clusters at many places and their presence within grains was minimal but visible (Figure 1). Matrix-reinforcement interfacial integrity was good as there was no evidence of debonding

or pores associated with CeO<sub>2</sub> particles. The porosity was typically not visible except for some isolated areas. This was consistent with the density measurement results and porosity computation, which revealed that in all the samples the porosity remained  $\leq 1\%$  (Table 1).

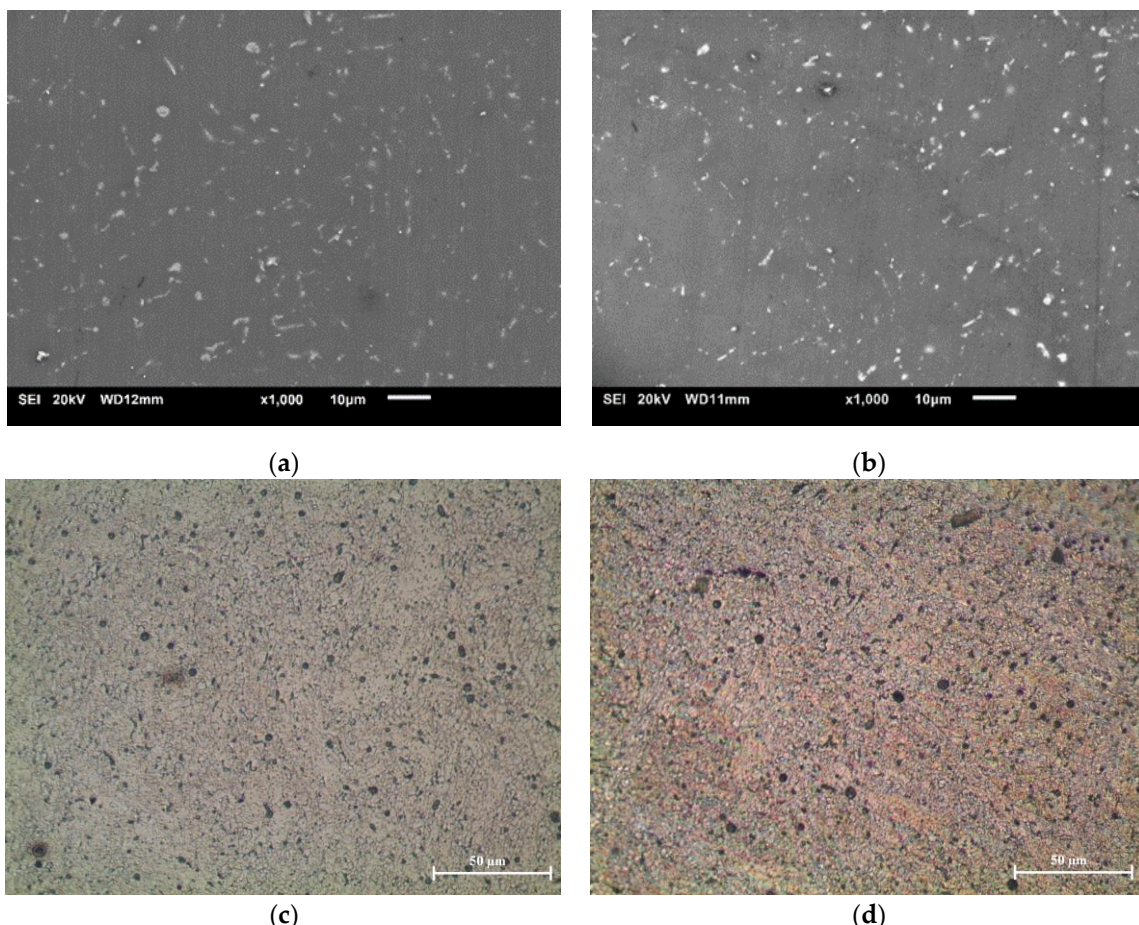


**Figure 1.** SEM micrographs showing the global distribution of ceria particles in (a) as-extruded and (b) as-extruded + DCT Mg/2wt.%CeO<sub>2</sub> samples. Optical micrograph of (c) as-extruded and (d) as extruded + DCT Mg/2wt.%CeO<sub>2</sub> samples.

The results of the XRD investigation are shown in Figure 2 in the longitudinal direction. A minimal presence or absence of oxides (MgO) and interfacial reaction products is anticipated as their peaks were not detected. Furthermore, all the peaks presented in Figure 2 are attributed to  $\alpha$ -Mg peaks as the amount of CeO<sub>2</sub> is  $\leq 2\%$ , which becomes undetectable in the X-ray analysis. The crystal structure of magnesium is HCP. Owing to this crystal structure of Mg, the deformation of magnesium is complicated to understand as there are multiple slip systems. The prismatic, basal, and pyramidal planes are the three most prominent slip systems, with the basal slip being the most prominent one. For pure Mg and Mg-based materials, the critical resolved shear stress (CRSS) for basal slip is much lower than that for non-basal slip systems. The normalized intensity is the ratio of the intensity corresponding to a particular 2Theta angle and the maximum intensity of the sample. The results reveal the maximum intensity for the basal plane ( $34^\circ$ ) followed by pyramidal ( $36^\circ$ ) and prismatic planes ( $32^\circ$ ) (Figure 1b) with strong basal texture both before and after DCT. The relative prismatic and pyramidal peak intensities were reduced following the DCT treatment. As the X-ray analysis is arbitrary in nature, for a better understanding and comparison of the influence of DCT, normalized intensities are presented. Figure 2b indicates that normalized intensities of both prismatic and pyramidal planes reduce after DCT. This indicates that DCT on Mg-CeO<sub>2</sub> nanocomposites is capable of altering the texture. Altering the texture

in magnesium-based materials is known to improve the plastic deformation capabilities of the material. Post-recrystallization during hot extrusion, the altering of texture can be a consequence of higher  $\langle c+a \rangle$  dislocation activity and refined grain size owing to the pinning of  $\text{CeO}_2$  particles along the grain boundaries [20].

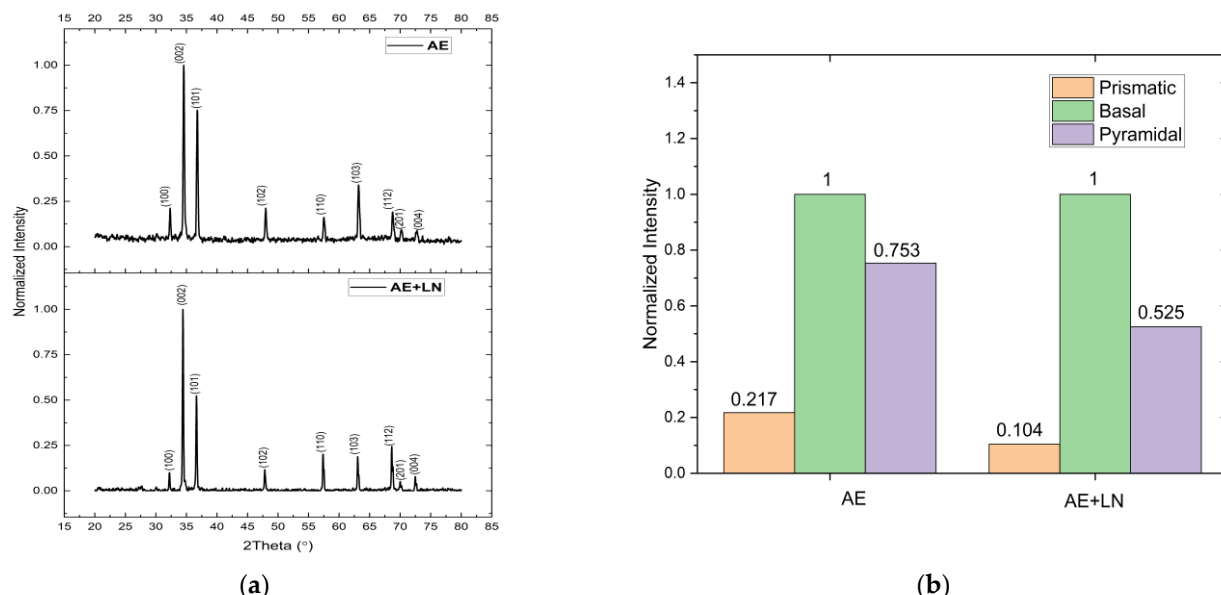


**Figure 2.** XRD results, taken in the longitudinal direction of the Mg/2wt.% $\text{CeO}_2$  samples. (a) Normalized XRD diffractograms; (b) The intensities of prismatic, basal and pyramidal planes.

### 3.4. Thermal Response

DSC studies (Figure 3) and ignition temperature (Table 3) measurements were conducted on the samples before and after DCT. DSC studies revealed a peak at approx. 470 °C indicating the release of stresses stored during DCT. As the matrix is pure Mg with no alloying elements, precipitation and dissolution are ruled out. For samples without DCT, no such peak was observed. The results indicate that compressive stresses will remain in the materials at ambient temperature and beyond and will influence the properties, typically mechanical properties, and may also lead to an enhancement in the fatigue response as introducing compressive stresses in the materials is one of the established ways to delay fatigue failure. Further work is required in this area to clearly understand at what critical temperature the material can retain these compressive stresses that have originated due to DCT treatment.

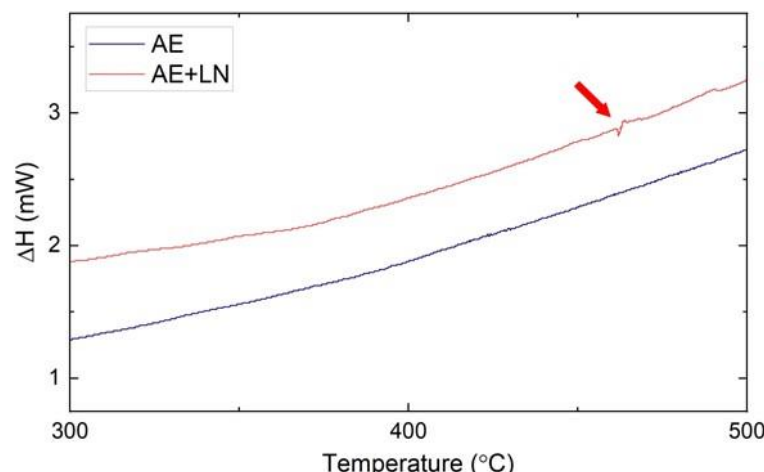


**Figure 3.** DSC results of samples with and without DCT.

**Table 3.** Results of ignition temperature measurements.

Material	Ignition Temperature (°C)
Pure Mg	580
Mg/2wt.%CeO <sub>2</sub> (AE)	665
Mg/2wt.%CeO <sub>2</sub> (AE + LN)	674

The results of ignition temperature measurements indicate an increase in ignition temperature by 12 °C (1.8%) when compared to the non-DCT sample. This may be attributed to the decrease in thermal conductivity of the sample due to defect generation (dislocations) during DCT. It has been established experimentally that the addition of ceramic reinforcements, which decreases the thermal conductivity, assists in increasing the ignition temperature (see Table 3 for a comparison between Mg and Mg/2wt.%CeO<sub>2</sub>) [21]. Additionally, it was noted that DCT leads to an increase in dislocation density and the capability of dislocations to scatter phonons is well-established, which reduces thermal conductivity [22]. Further, deep cryogenic treatment of the as-extruded nanocomposite sample led to a reduction in porosity by ~44%. The reduction in porosity can be linearly linked with the improvement in thermal stability and increase in the ignition temperature as the lesser the porosity, the lesser the sites of auto-ignition in the material. This facilitates a delay in the onset of ignition, thereby improving the ignition temperature of the material post-DCT.

### 3.5. Mechanical Response

The mechanical response in this study was assessed from hardness (Table 4) and compression testing (Figure 4 and Table 5). Microhardness characterization was carried out as it is an excellent indicator of the response of the material in different tribological (sliding) conditions. Notably, metal-based composites are often used in sliding applications, particularly in the automotive sector and for erosion resistance such as in hydrothermal power stations. The increase in microhardness was 7% following DCT, indicating the crucial role of the increase in dislocation density and compressive stresses that are stored in materials during DCT [1,8,14,17]. Among these two factors, an increase in dislocation density that reflects an increase in the number of dislocations per unit area will be more dominant as these dislocations will obstruct the motion of dislocations during localized plastic deformation during indenter penetration. Further, the increase in hardness of DCT samples can be attributed to the decrease in porosity following DCT (1.099 to 0.5545–50%). The role of grain size can be ignored as there was no statistical difference.

**Table 4.** Results of microhardness measurements.

Material	Microhardness (HV)
Pure Mg <sup>a</sup>	55 ± 3
Mg/2wt.%CeO <sub>2</sub> (AE)	86 ± 2
Mg/2wt.%CeO <sub>2</sub> (AE + LN)	92 ± 4 (↑7%)

<sup>a</sup> Values generated in the laboratory using similar raw materials and processing methods [16].

As the magnesium-based materials typically have an HCP crystal structure and display limited ductility, they are used in most scenarios where the primary form of load-bearing is under the compressive mode. Hence, from a design standpoint, improving the compressive properties is of utmost importance as compared to tensile tests for Mg-based materials and, therefore, this has been investigated in this study as a priority. The results of compressive testing in this study revealed an increase in 0.2% CYS (18%), fracture strain (43%), and energy absorbed until failure by 46% (Figure 4 and Table 5). The drop in UCS was marginal (1.3%) and can be ignored as it was statistically insignificant. The increase in CYS can be primarily attributed to an increase in dislocation density during DCT, as the grain size difference between DCT and non-DCT samples was insignificant and the matrix was pure

magnesium so the effect of enhanced precipitation as reported in other studies can be ruled out. The increase in ductility (43%) was perhaps the most intriguing in this work. The increase in ductility following cryogenic treatment of magnesium-based alloys can be attributed to [14]: (a) the reduction in grain size; (b) the presence of twins as they allow the magnesium alloys to adjust to plastic deformation; and (c) texture weakening. In the case of nanocomposites, none of these factors was available to increase the ductility and the increase can only be attributed to (a) the enhanced density of the matrix (reduction in porosity by ~50%, as pores can serve as crack nucleation sites under loading); (b) enhanced matrix-reinforcement interfacial bonding due to the contraction of metallic matrix against the ceramic particulates; and (c) an increase in quantum of compressive stresses due to DCT. Figure 5 shows the schematic of the mechanism of enhanced matrix-reinforcement interfacial bonding as a result of DCT. The as-cast material following solidification typically shows matrix-reinforcement debonded areas (Figure 5a). Following extrusion, the porosity is minimized in the matrix and matrix-reinforcement interfacial bonding improves due to the action of shear and compressive stresses during the extrusion process (Figure 5b). When extruded samples are subjected to DCT, compressive stresses are further introduced, which enhances the matrix-reinforcement interfacial integrity further (Figure 5c). The enhancement in Mg/CeO<sub>2</sub> interfacial bonding and the presence of increased compressive stresses are instrumental in delaying particulate-related damage mechanisms (particulate cracking and particulate debonding), in this case, matrix-reinforcement interfacial debonding, leading to enhanced ductility.

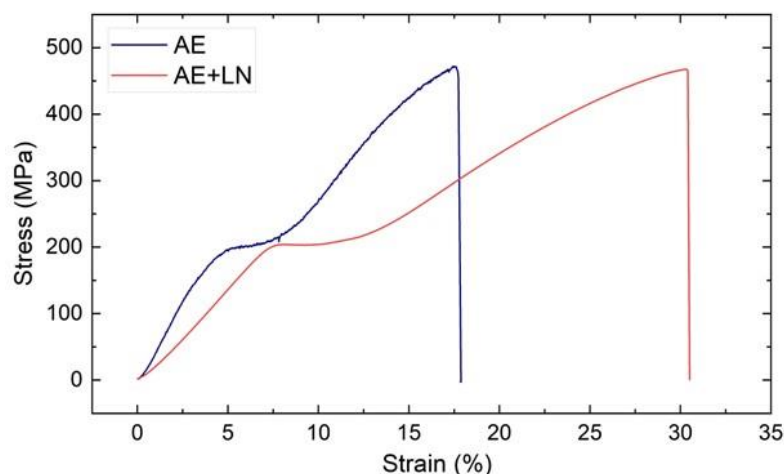


**Figure 4.** Compressive stress–strain curves of samples with and without DCT.

**Table 5.** Results of compressive testing results.

Material	0.2% CYS (MPa)	UCS (MPa)	Fracture Strain (%)	Energy Absorbed (MJ·mm <sup>-3</sup> )
Pure Mg <sup>a</sup>	63 ± 4	278 ± 5	24 ± 1	45
Mg/2wt.%CeO <sub>2</sub> (AE)	174 ± 18	458 ± 25	21 ± 6	52
Mg/2wt.%CeO <sub>2</sub> (AE + LN)	206 ± 3 (↑18%)	452 ± 15	30 ± 1 (↑43%)	76 (↑46%)
Mg-2Nd-4Zn <sup>a</sup>	242	502	8	-
AZ31 <sup>b</sup>	-	250	28	-
WE43 <sup>b</sup>	261	420	16.3	-
AM50 <sup>b</sup>	104	296	12.6	-
ZK60 <sup>b</sup>	159	472	12.4	-
AZ91D <sup>b</sup>	130	300	12.4	-
ME21 <sup>b</sup>	87	260	25	-

<sup>a</sup>—Cryogenic treatment in liquid nitrogen (77 K) for 1 day [7]; <sup>b</sup>—Extruded magnesium alloys [23].

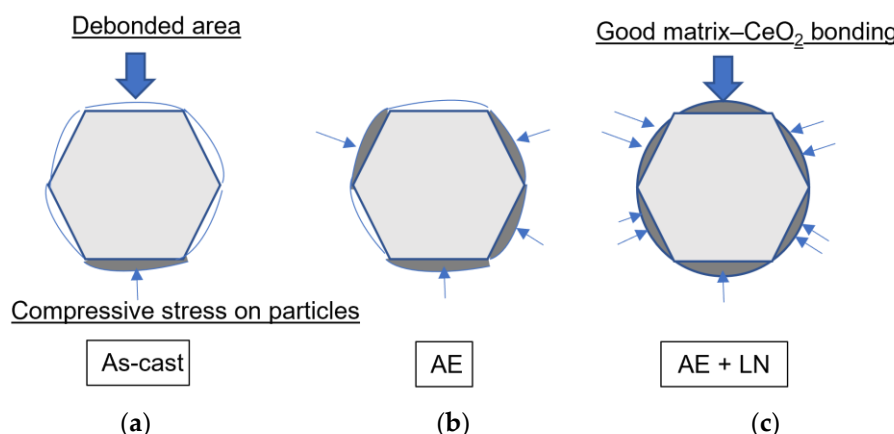


**Figure 5.** Schematic diagram showing the improvement in Mg/CeO<sub>2</sub> interfacial bonding and increase in quantum of compressive stresses from (a) as-cast; (b) extruded; (c) DCT-treated samples. The greater the number of arrows, the greater the quantum of compressive stresses.

The fractographs taken from compressively fractured samples for both the as-extruded and DCT-treated samples revealed cleavage-type fractures typical of magnesium-based materials (Figure 6). In both cases, shear bands were observed. The fracture surface in the case of the DCT-treated sample was rougher when compared to the as-extruded sample suggesting more crack meandering consistent with an increase in ductility (see Table 5).

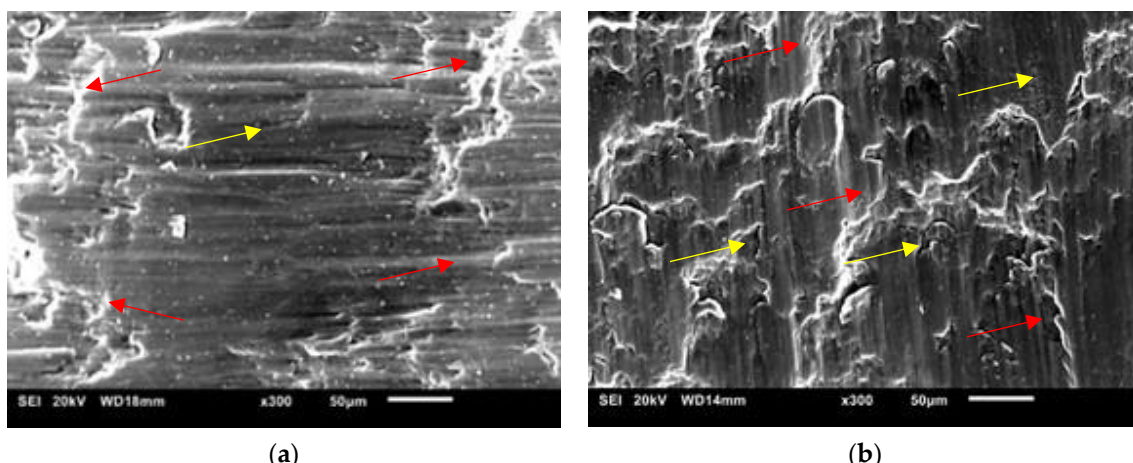


**Figure 6.** Fractographs of (a) as-extruded and (b) as-extruded + DCT Mg/2wt.%CeO<sub>2</sub> samples. The red arrows indicate the shear bands, and the yellow arrows indicate the microcracks.

#### 4. Conclusions

Magnesium-cerium oxide nanocomposite developed using disintegrated melt deposition followed by extrusion was exposed to liquid nitrogen treatment. The key findings of the study are summarized below.

- Exposure to liquid nitrogen (77 K) assists in reducing the porosity of the nanocomposite samples by ~44%.
  - Grain size analysis revealed that the extrusion process reduced the grain size from 22  $\mu\text{m}$  of DMD-solidified material to 2  $\mu\text{m}$ , which remained similar following DCT treatment.
  - DCT treatment was effective in reducing the porosity by approximately 43%. The porosity was measured, in this case, before and after DCT on the same samples.
  - The ignition temperature of the nanocomposite post-DCT is observed to be ~9 °C higher than the as-extruded sample.
  - DCT treatment was effective in improving the hardness from 86 HV to 92 HV (~7%).

- There was a superior improvement in the compressive yield strength (18%) and fracture strain (43%) values post-DCT with no adverse effect on the ultimate compressive strength.

**Author Contributions:** Conceptualization, G.P. and M.G.; methodology, M.G.; validation, S.G., G.P. and K.S.T.; formal analysis, S.G., G.P., K.S.T. and M.G.; investigation, S.G., G.P. and K.S.T.; resources, M.G.; data curation, S.G., G.P. and K.S.T.; writing—original draft preparation, S.G., G.P. and M.G.; writing—review and editing, S.G., G.P. and M.G.; visualization, S.G. and G.P.; supervision, G.P., K.S.T. and M.G.; project administration, M.G.; funding acquisition, M.G. All authors have read and agreed to the published version of the manuscript.

**Funding:** This research was funded by the Singapore Ministry of Education, Tier 1, grant number R-265-000-684-114 (A-000523401-00) and the APC was funded by R-265-000-684-114 (A-000523401-00).

**Data Availability Statement:** Data will be made available on request.

**Conflicts of Interest:** The authors declare no conflict of interest. The funders had no role in the design of the study; in the collection, analyses, or interpretation of data; in the writing of the manuscript; or in the decision to publish the results.

## References

1. Sonar, T.; Lomte, S.; Gogte, C. Cryogenic Treatment of Metal—A Review. *Mater. Today Proc.* **2018**, *5*, 25219–25228. [[CrossRef](#)]
2. Dieringa, H. Influence of Cryogenic Temperatures on the Microstructure and Mechanical Properties of Magnesium Alloys: A Review. *Metals* **2017**, *7*, 38. [[CrossRef](#)]
3. Baldissera, P.; Delprete, C. Deep cryogenic treatment: A bibliographic review. *Open Mech. Eng. J.* **2008**, *2*, 1–11. [[CrossRef](#)]
4. Das, D.; Ray, K.K.; Dutta, A.K. Influence of temperature of sub-zero treatments on the wear behaviour of die steel. *Wear* **2009**, *267*, 1361–1370. [[CrossRef](#)]
5. Barron, R.F. Cryogenic treatment of metals to improve wear resistance. *Cryogenics* **1982**, *22*, 409–413. [[CrossRef](#)]
6. Shunmuga Priyan, M. Optimization of Retained Austenite and Corrosion Properties on EN-31 Bearing Steel by Cryogenic Treatment Process; IntechOpen: Rijeka, Croatia, 2022.
7. Dong, N.; Sun, L.; Ma, H.; Jin, P. Effects of cryogenic treatment on microstructures and mechanical properties of Mg-2Nd-4Zn alloy. *Mater. Lett.* **2021**, *305*, 130699. [[CrossRef](#)]
8. Jiang, Y.; Chen, D.; Chen, Z.; Liu, J. Effect of Cryogenic Treatment on the Microstructure and Mechanical Properties of AZ31 Magnesium Alloy. *Mater. Manuf. Process.* **2010**, *25*, 837–841. [[CrossRef](#)]
9. Lin, T.; Zhou, J.-X.; Jing, C.-N.; Liu, Y.-T.; Zhang, L.-L.; Meng, X.-B. Improving mechanical properties of ZK60 magnesium alloy by cryogenic treatment before hot extrusion. *High Temp. Mater. Process.* **2020**, *39*, 200–208. [[CrossRef](#)]
10. Stephens, T.; Birk, A.; Gohlke, D. Vehicle Technologies and Fuel Cell Technologies Office Research and Development Programs: Prospective Benefits Assessment Report for Fiscal Year 2018; Argonne National Lab. (ANL): Argonne, IL, USA, 2017.
11. Kawajiri, K.; Kobayashi, M.; Sakamoto, K. Lightweight materials equal lightweight greenhouse gas emissions: A historical analysis of greenhouse gases of vehicle material substitution. *J. Clean. Prod.* **2020**, *253*, 119805. [[CrossRef](#)]
12. Gonçalves, M.; Monteiro, H.; Iten, M. Life Cycle Assessment studies on lightweight materials for automotive applications-An overview. *Energy Rep.* **2022**, *8*, 338–345. [[CrossRef](#)]
13. Gupta, M.; Sharon, N.M.L. *Magnesium, Magnesium Alloys, and Magnesium Composites*; John Wiley & Sons: Hoboken, NJ, USA, 2011.
14. Huang, H.; Zhang, J. Microstructure and mechanical properties of AZ31 magnesium alloy processed by multi-directional forging at different temperatures. *Mater. Sci. Eng. A* **2016**, *674*, 52–58. [[CrossRef](#)]
15. Kumar Meenashisundaram, G.; Hou Damien Ong, T.; Parande, G.; Manakari, V.; Xiang, S.; Gupta, M. Using lanthanum to enhance the overall ignition, hardness, tensile and compressive strengths of Mg-0.5Zr alloy. *J. Rare Earths* **2017**, *35*, 723–732. [[CrossRef](#)]
16. Parande, G.; Tun, K.S.; Neo, H.J.N.; Gupta, M. An Investigation into the Effect of Length Scale (Nano to Micron) of Cerium Oxide Particles on the Mechanical and Flammability Response of Magnesium. *J. Mater. Eng. Perform.* **2022**. [[CrossRef](#)]
17. Tsai, M.; Chang, C. Grain size effect on deformation twinning in Mg-Al-Zn alloy. *Mater. Sci. Technol.* **2013**, *29*, 759–763. [[CrossRef](#)]
18. Fan, H.; Aubrey, S.; Arsenlis, A.; El-Awady, J.A. Grain size effects on dislocation and twinning mediated plasticity in magnesium. *Scr. Mater.* **2016**, *112*, 50–53. [[CrossRef](#)]
19. Arul Kumar, M.; Beyerlein, I.J.; Tome, C.N. Grain size constraints on twin expansion in hexagonal close packed crystals. *J. Appl. Phys.* **2016**, *120*, 155105. [[CrossRef](#)]
20. Mishra, R.K.; Brahme, A.; Sabat, R.K.; Jin, L.; Inal, K. Twinning and texture randomization in Mg and Mg-Ce alloys. *Int. J. Plast.* **2019**, *117*, 157–172. [[CrossRef](#)]
21. Manakari, V.; Parande, G.; Doddamani, M.; Gupta, M. Enhancing the Ignition, Hardness and Compressive Response of Magnesium by Reinforcing with Hollow Glass Microballoons. *Materials* **2017**, *10*, 997. [[CrossRef](#)] [[PubMed](#)]

22. Kogure, Y.; Hiki, Y. Effect of dislocations on low-temperature thermal conductivity and specific heat of copper-aluminum alloy crystals. *J. Phys. Soc. Jpn.* **1975**, *39*, 698–707. [[CrossRef](#)]
23. Parande, G.; Joju, J.; Manakari, V.; Teo, Z.M.B.; Gupta, M. An experimental investigation on the influence of hybrid turning induced deformation parameters on the properties of Mg-Zn-Sr-Dy alloy. *J. Mater. Process. Technol.* **2023**, *312*, 117845. [[CrossRef](#)]

**Disclaimer/Publisher's Note:** The statements, opinions and data contained in all publications are solely those of the individual author(s) and contributor(s) and not of MDPI and/or the editor(s). MDPI and/or the editor(s) disclaim responsibility for any injury to people or property resulting from any ideas, methods, instructions or products referred to in the content.